e-ISSN 2320 –7876 www.ijfans.org
Research Paper
Vol.11, Iss.9, Dec 2022

Synthesis and magnetic properties of spinel Mn-Mg ferrite nanoparticles for catalytic applications

M. Malarpriya[1,*], G. Padma Priya[1]
[1] Department of Chemistry, Faculty of Arts and Science,
Bharath Institute of Higher Education and Research (BIHER),
Chennai – 600073, Tamil Nadu, India
***Corresponding Author Email:** malarpriyaa57@gmail.com (M. Malarpriya)

Address for Correspondence

M. Malarpriya[1,*], G. Padma Priya[1]
[1] Department of Chemistry, Faculty of Arts and Science,
Bharath Institute of Higher Education and Research (BIHER),
Chennai – 600073, Tamil Nadu, India
***Corresponding Author Email:** malarpriyaa57@gmail.com (M. Malarpriya)

Abstract

Magnetically separable spinel Mn-$MgFe_2O_4$ NPs was synthesized by a facile microwave-assisted combustion method. The formation of single-phase cubic spinel structure was confirmed by XRD, FT-IR and EDX analyses. The energy band gap of the samples was confirmed by UV-Vis DRS study and the band gap of pure $MgFe_2O_4$ sample is 2.17 eV and it is increased with increasing the amount of Mn^{2+} dopant, due to the decrease of particle size. VSM showed ferromagnetic behavior for all compositions.

Keywords: Mn-$MgFe_2O_4$ NPs; combustion method; ferromagnetic behavior.

1. Introduction

As one of the families of transition metal oxides, spinel-type magnetic materials with the general formula $M^{2+}(Fe^{3+})_2O_4$: where M^{2+} = Mn^{2+}, Co^{2+}, Mg^{2+}, Zn^{2+}, etc. have become an important area in nano-science and nanotechnology, due to their huge applications in various field such as biomedicine, magnetic materials, electronic materials, and photo-catalysts [1,2].

Among various spinel ferrites, magnesium ferrite ($MgFe_2O_4$) nanostructures have been widely used in different fields such as, catalytic, and gas sensors [3-5]. Several methods has been used to prepare $MgFe_2O_4$ nanomaterials such as polymer calcinations laser deposition, co-precipitation and solvothermal [6-10] methods. However, the above methods reveal that requirement of complicated equipment, high-energy consuming, high temperature, long time consuming and complex procedures are required for synthesis of such functional materials. Hence, the growth of simple and environmentally benign synthesis methods is strictly essential and preferred with low energy cost [11-25].

In the present study, we have reported a facile microwave-assisted combustion method for the synthesis of spinel $MgFe_2O_4$ nanostructures. This method is fundamentally different from other conventional methods, due to the homogeneous distribution of microwave energy through the materials interior and converted into the final product within few minutes of time [26-30].

2. Experimental

2.1. Materials and methods

All the chemicals used in this study were of analytical grade obtained from Merck, India and were used as received without further purification. Magnesium nitrate ($Mg(NO_3)_2{\cdot}6H_2O$, 98%), manganese nitrate ($Mn(NO_3)_2{\cdot}4H_2O$, 98%), ferric nitrate ($Fe(NO_3)_3{\cdot}9H_2O$, 98%) and urea ($CO(NH_2)_2$) as the fuel are used for this combustion method. The samples were prepared with the addition of Mn^{2+} of different molar ratios (Mn-$MgFe_2O_4$) to $MnFe_2O_4$. In case of $MnFe_2O_4$, the precursor mixture in urea was placed in a domestic microwave oven and exposed to the microwave energy in a 2.45 GHz multimode cavity at 850W for 10 minutes. Initially, the precursor mixture boiled and underwent evaporation followed by the decomposition with the evolution of gases. When the solution reached the point of spontaneous combustion, it vaporized and instantly became a solid and then used for further characterizations.

2.2. Characterizations

The structural characterization of Mn-$MgFe_2O_4$ NPs were performed using a Philips PANanalytical X' pert PRO diffractometer equipped with a Cu tube for generating a Cu Kα radiation (wavelength 1.5406 Å) at 40 kV, 25 mA. Structural refinements using the Rietveld method was carried out by PDXL program; both refined lattice parameters and crystallite size of the obtained ferrites were reported. The surface functional groups were analyzed by Thermo Nickolet FT-IR spectrometer. The samples were incorporated in KBr pellets for the measurements. Morphological studies and energy dispersive X-ray analysis of Mn-$MgFe_2O_4$ have been performed with a Jeol JSM6360 high resolution scanning electron microscopy. The transmission electron micrographs were carried out by Philips-TEM (CM20). The surface area was derived from the N_2 adsorption-desorption isotherms using liquid nitrogen at 77 K using an automatic adsorption instrument (Quantachrome Corp. Nova-1000 gas sorption analyzer). The UV-Visible diffuse reflectance spectrum was recorded using Varian Cary 5E UV/VIS-NIR UV-Visible spectrophotometer to estimate their band gap energy (E_g). The photoluminescence properties were recorded at room temperature using Perkin Elmer LS 55 Fluorescence Spectrophotometer. Magnetic measurements were carried out at room temperature using a PMC MicroMag 3900 model vibrating sample magnetometer (VSM) equipped with 1 Tesla magnet.

3. Results and discussion

3.1. Structural analysis

The structural phase, crystalline nature and purity of the prepared $Mn_xMg_{1-x}Fe_2O_4$ NPs were confirmed by analyzing the X-ray powder diffraction (XRD) patterns. Fig. 1 shows the XRD patterns of Mn-$MgFe_2O_4$ NPs prepared with various Mn substitutions. The main diffraction peaks (2θ) are attributed to the (220), (311), (222), (400), and (533) planes, respectively show the characteristics of a single-phase cubic spinel structure with Fd3m space group (JCPDS No. 73-1722) [23] and all diffraction peaks can be indexed to a typical spinel structured $MgFe_2O_4$. The observed

e-ISSN 2320 –7876 www.ijfans.org
Vol.11, Iss.9, Dec 2022

Research Paper

diffraction peaks indicates well defined spinel phase, which was developed during the combustion. The average crystallite size of $Mn_xMg_{1-x}Fe_2O_4$ samples was calculated by using Debye Scherrer formula,

$$L = \frac{0.89\lambda}{\beta \cos\theta} \qquad \text{------ (1)}$$

where *'L'* is the average crystallite size, *'λ'*, the X-ray wavelength (1.5406 Å), *'β'*, full width at half maximum (FWHM) and *'θ'*, the Bragg angle of the (311) plane It has been observed that the crystallite size is decreased from 25.25-15.55 nm with increase in Mn content [24, 25].

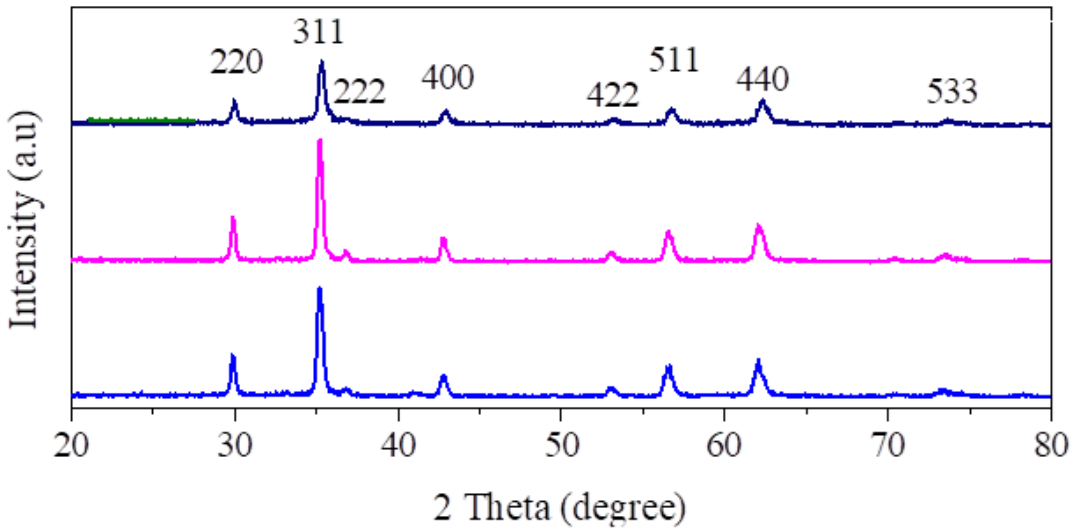

Figure 1. XRD patterns of Mn-$MgFe_2O_4$ (x = 0.0, 0.3 and 0.5) NPs.

In order to further analyze the structural change, the measured XRD patterns of the NPs were simulated based on the Rietveld refinement method for all compositions. Fig. 2 shows the Rietveld XRD data of $MgFe_2O_4$ and $Mn_{0.5}Mg_{0.5}Fe_2O_4$ NPs respectively. Rietveld XRD was designed to refine simultaneously both lattice constant and crystallite size. The lattice parameter of pure $MgFe_2O_4$ is 8.385 Å [26] and it is increased with increasing Mn content from 8.395 to 8.435 Å, thus obeying Vegard's law. However, the increase of lattice parameter is mainly due to the higher

ionic radius of Mn^{2+} ion (0.91 Å) than smaller ionic radius of Mg^{2+} ion (0.65 Å), and thus causes an effective increase in the lattice constant. A linear increase in the lattice constant indicates that Mn ions are replacing Mg ions in $MgFe_2O_4$ matrix [27, 28].

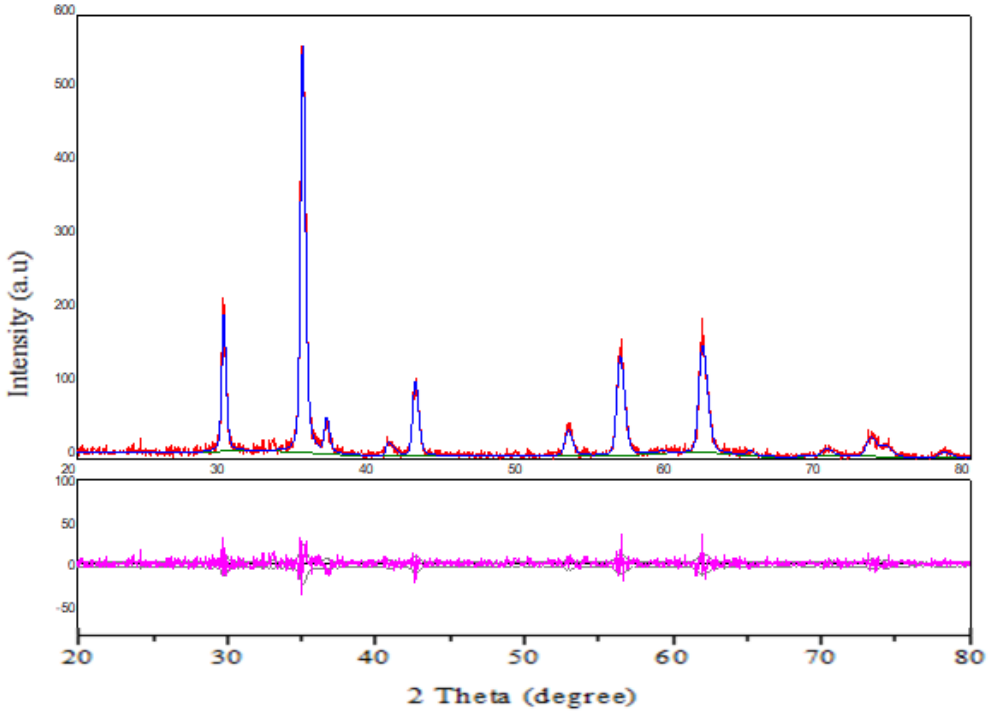

Figure 2. Rietveld refinement XRD method of Mn-$MgFe_2O_4$ (x = 0.5) NPs.

3.2. Fourier transform infrared (FT-IR) spectroscopy

FT-IR spectra of Mn-$MgFe_2O_4$ NPs are shown in Fig. 3. From the FT-IR spectra, it is found that two strong absorption peaks observed at lower frequency can be assigned to the M-O (Mg, Mn and Fe) bonds at tetrahedral (A) and octahedral (B) sites [29]. This can be attributed to the high degree of crystalline Mn-$MgFe_2O_4$ NPs. The obtained results were good agreement with Rietveld refinement XRD analysis. The aforementioned two peaks also confirmed the formation of tetrahedral and octahedral structures [24].

e-ISSN 2320 –7876 www.ijfans.org
Research Paper
Vol.11, Iss.9, Dec 2022

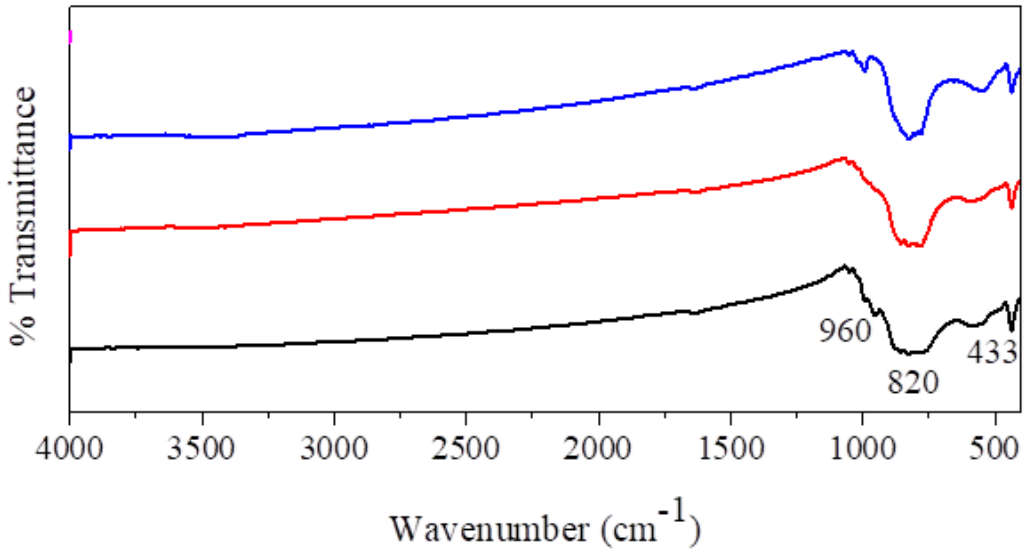

Figure 3. FT-IR analysis of Mn-$MgFe_2O_4$ (x = 0.3, 0.4 and 0.5) NPs.

3.3. Scanning electron microscopy (SEM) studies

The morphologies of Mn-$MgFe_2O_4$ NPs were investigated by the high resolution scanning electron microscopy (HR-SEM) and the obtained results are shown in Fig. 4.. HR-SEM images indicated that the as-prepared samples consist of spherical shaped particle-like nanocrystals, which are agglomerated together, due to the presence of magnetic interactions among the particles [25].

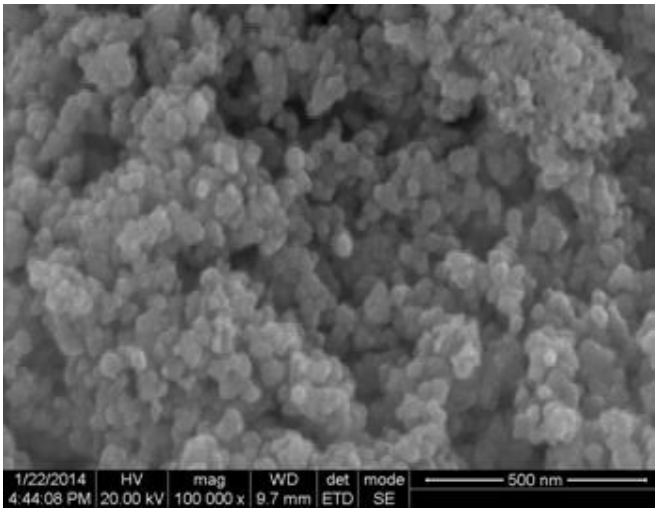

Figure 4. HR-SEM images of $Mn_{0.5}Mg_{0.5}Fe_2O_4$ NPs.

e-ISSN 2320 –7876 www.ijfans.org
Research Paper
Vol.11, Iss.9, Dec 2022

3.4. Transmission electron microscopy (TEM) studies

To provide a further evidence for the formation of sphere-like nanoparticle morphology of Mn-$MgFe_2O_4$ NPs, HR-TEM analysis was carried out and is shown in Fig. 5. HR-TEM image of Mn-$MgFe_2O_4$ NPs sphere-like nanoparticles with diameter ranging from 25-30 nm. It is obvious that the sphere-like nanoparticles are uniform in size, which is consistent with the average crystallite size obtained from the peak broadening in XRD and Rietveld analysis. Fig. 6 inset shows the SAED of spinel Mn-$MgFe_2O_4$ NPs, which implies that the as-prepared samples are single crystalline in nature. SAED results show spotty ring characteristic of small crystallites of spinel ferrite nanostructure without any additional diffraction spots and rings of secondary phases corresponding to the magnesium, manganese and iron oxides were observed.

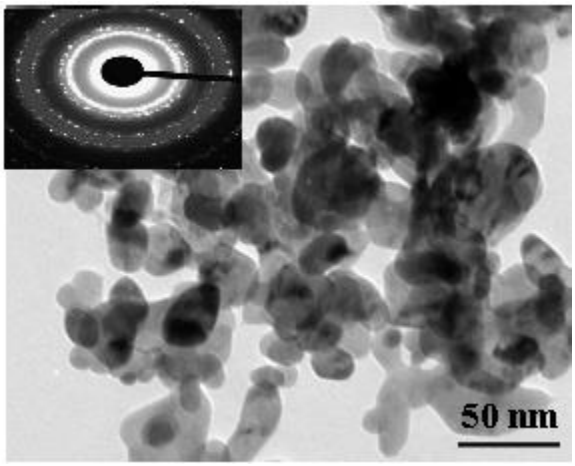

Figure 5. HR-TEM images of $Mn_{0.5}Mg_{0.5}Fe_2O_4$ NPs.

3.5. EDX analysis

The elemental composition and purity of the samples were recorded by EDX analysis. Fig. 6 shows the EDX results of Mn-$MgFe_2O_4$ NPs, and there is no other peaks, which is confirmed the as-prepared samples are pure and there is no other impurity.

e-ISSN 2320 –7876 www.ijfans.org
Vol.11, Iss.9, Dec 2022

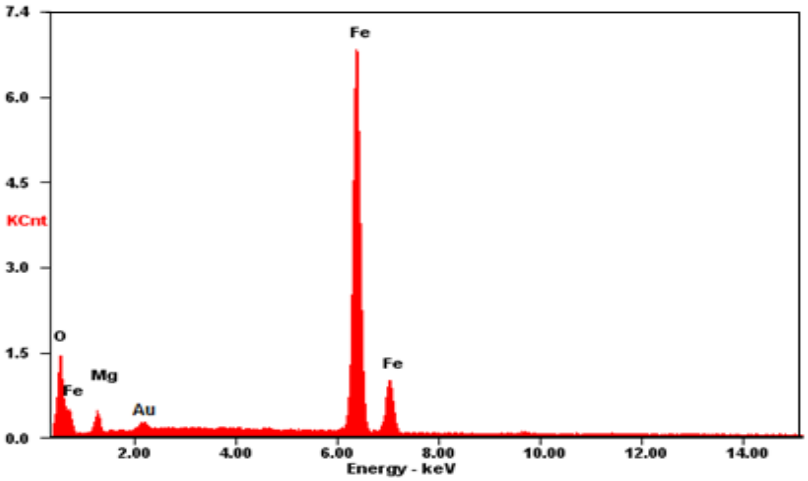

Figure 6. EDX spectra of $MgFe_2O_4$ NPs.

3.6. UV-Vis DRS study

To study the effect of crystallite size on optical property of spinel Mn-$MgFe_2O_4$ NPs, the UV-Visible diffuse reflectance spectroscopy (DRS) analysis was carried out at room temperature for all compositions. The band gap energy E_g, can be approximately calculated from the optical diffuse reflectance data by the Kubelka-Munk function,

$$F(R) = (1-R)^2 /2R \qquad \text{------ (2)}$$

where *'R'* is the diffuse reflectance. A graph is plotted between $[F(R)h\upsilon]^2$ and $h\upsilon$, and the intercept obtained is the band gap energy, indicating that the $MgFe_2O_4$ NPs may have visible-light photoactivity. The shift in E_g of the Mn-$MgFe_2O_4$ NPs with the decreasing crystallite size is the result of quantum confinement effects arising from the small size regime [26-30].

e-ISSN 2320 –7876 www.ijfans.org
Research Paper
Vol.11, Iss.9, Dec 2022

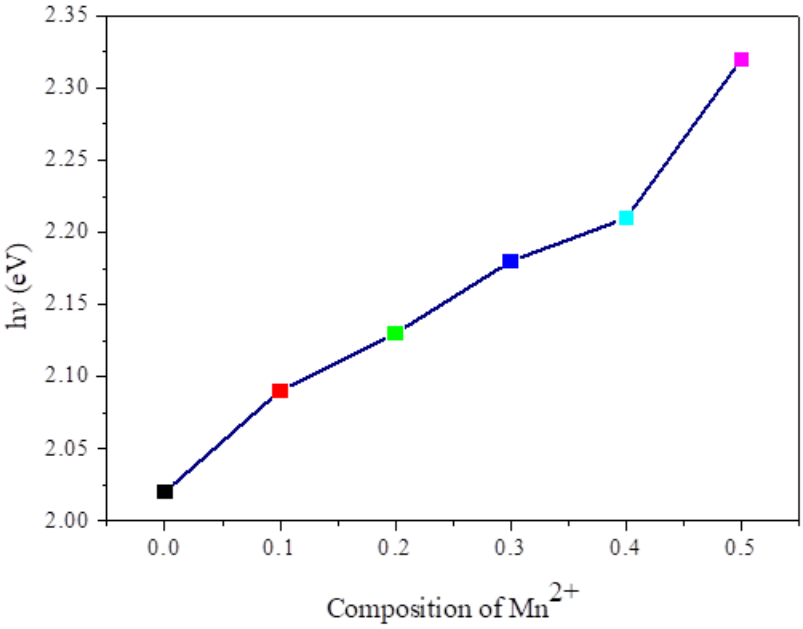

Figure 7. UV-Vis DRS band gap of Mn-$MgFe_2O_4$ NPs.

3.7. Photoluminescence (PL) studies

Photoluminescence (PL) spectroscopy is an effective method to study the electronic, optical and photochemical properties of the metal oxides. PL spectra was recorded at room temperature to detect the optical properties of Mn-$MgFe_2O_4$ NPs and are shown in Fig. 9 is attributed to the recombination of electrons deeply trapped in oxygen vacancies with photo-generated holes [26-31]. The increase of the concentration of Mn^{2+} dopant into $MgFe_2O_4$, overall intensities of the PL peak for all compositions decreases, which can be attributed to the appearance of new electronic levels between conduction and valence band and might be due to the increase in intrinsic defects.

e-ISSN 2320 –7876 www.ijfans.org
Vol.11, Iss.9, Dec 2022

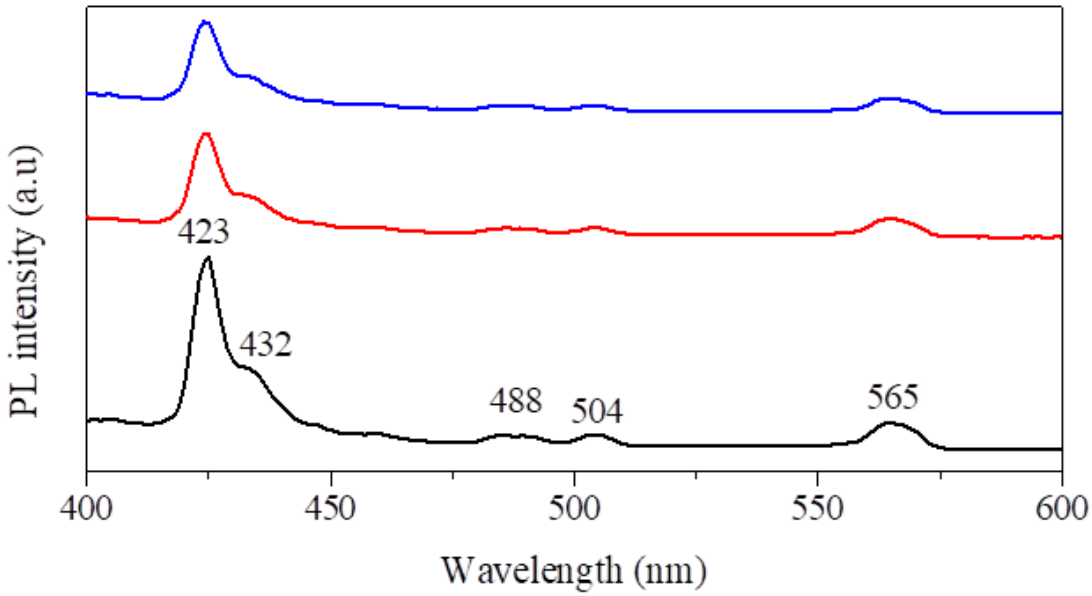

Figure 8. PL spectra of Mn-$MgFe_2O_4$ (x = 0.3, 0.4 and 0.5) NPs.

3.8 Magnetic measurements

The magnetic hysteresis (M-H) curves of the spinel Mn-$MgFe_2O_4$ NPs obtained from room temperature VSM measurement with the applied field ranging from -10000 to +10000 O_e is shown in Fig. 9, which clearly indicated that the prepared Mn-$MgFe_2O_4$ NPs based photocatalyst can be separated from water by the application of external magnetic field [32-36]. These curves are typical for a soft magnetic material and indicate hysteresis ferromagnetism in the field ranges of ±10 KOe for all compositions. $MgFe_2O_4$ is a soft magnetic material and the non-magnetic Mn-$MgFe_2O_4$ NPs is substituted by magnetic Mn^{2+} ions, there is a drastic change in magnetic properties such as M_s, M_r and H_c. Outside these ranges the value of M_s increases with increasing the concentration of Mn^{2+}.

e-ISSN 2320 –7876 www.ijfans.org
Research Paper
Vol.11, Iss.9, Dec 2022

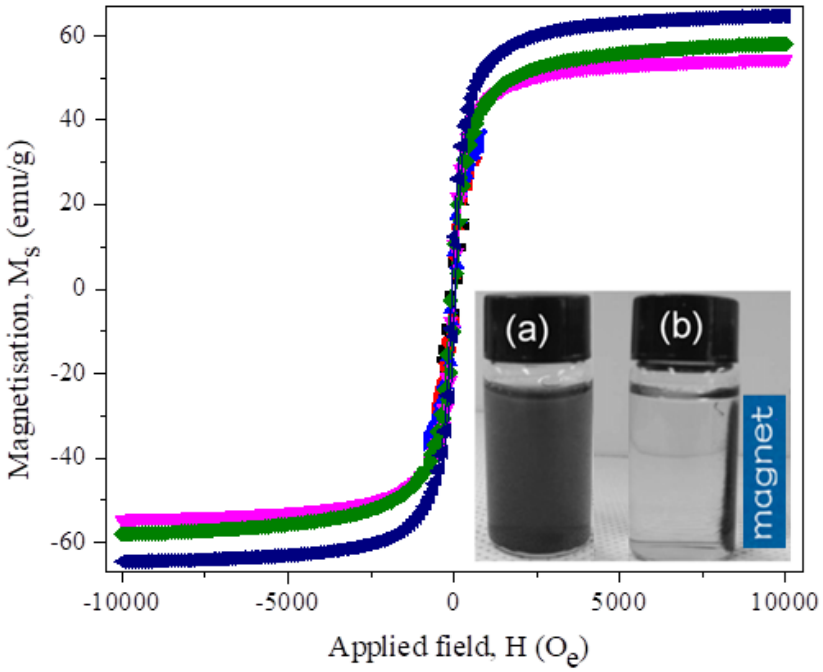

Figure 9. Magnetic hysteresis (M-H) loops of Mn-$MgFe_2O_4$ NPs.

4. Conclusions

Spinel Mn-$MgFe_2O_4$ NPs have been successfully synthesized by a facile, low-cost, microwave-assisted flash combustion route. It was found that the structural, morphological and opto-magnetic properties are sensitively dependent on the incorporation of Mn^{2+} ions in the Mg^{2+} lattice of $MgFe_2O_4$. On doping Mn^{2+} ions in $MgFe_2O_4$ lattice, the ferromagnetic behavior. The magnetization at the maximum field monotonically increases with increasing Mg content x = 0.5, which is attributed to the change in the cationic distribution at tetrahedral and octahedral sites. Smaller values of the coercivity showed the soft magnetic nature of these Mn-$MgFe_2O_4$ NPs.

References

[1]. M. A. Almessiere, Y. Slimani, H. Güngüneş, K. A. Demir, Z. Tatiana, T. Sergei, T. Alex, A. Manikandan, A. Fatimah, A. Baykal, Influence of Dy^{3+} ions on microstructure, magnetic, electrical and microwave properties of $[Ni_{0.4}Cu_{0.2}Zn_{0.4}](Fe_{2-x}Dy_x)O_4$ (0.00<x<0.04) spinel ferrites, ACS Omega, 6 (2021) 10266-10280.

[2]. P. Annie Vinosha, A. Manikandan, A. Christy Preetha, A. Dinesh, Y. Slimani, M.A. Almessiere, A. Baykal, Belina Xavier, G. Francisco Nirmala, Review on recent advances of synthesis, magnetic properties and water treatment applications of cobalt ferrite nanoparticles and nanocomposites, Journal of Superconductivity and Novel Magnetism, 34 (2021) 995–1018.

[3]. K. Elayakumar, A. Manikandan, A. Dinesh, K. Thanrasu, K. Kanmani Raja, R. Thilak Kumar, Y. Slimani, S. K. Jaganathan, A. Baykal, Enhanced magnetic property and antibacterial biomedical activity of Ce^{3+} doped $CuFe_2O_4$ spinel nanoparticles synthesized by sol-gel method, J. Magn. Magn. Mater. 478 (2019) 140–147.

[4]. A. Godlyn Abraham, A. Manikandan, E. Manikandan, S. Vadivel, S. K. Jaganathan, A. Baykal, P. Sri Renganathan, Enhanced magneto-optical and photo-catalytic properties of transition metal cobalt (Co^{2+} ions) doped spinel $MgFe_2O_4$ ferrite nanocomposites, J. Magn. Magn. Mater. 452 (2018) 380-388.

[5]. M. Maria Lumina Sonia, S. Anand, S. Blessi, S. Pauline, A. Manikandan, Effect of surfactants (PVB/EDTA/CTAB) assisted sol-gel synthesis on structural, magnetic and dielectric properties of $NiFe_2O_4$ nanoparticles, Ceram. Int. 44 (2018) 22068-22079.

[6]. K. Elayakumar, A. Dinesh, A. Manikandan, P. Murugesan, G. Kavitha, S. Prakash, R. Thilak Kumar, S. K. Jaganathan, A. Baykal, Structural, morphological, enhanced magnetic properties and antibacterial bio-medical activity of rare earth element (REE) Cerium (Ce^{3+}) doped $CoFe_2O_4$ nanoparticles, J. Magn. Magn. Mater. 476 (2019) 157-165.

[7]. Md Amir, H. Gungunes, A. Baykal, M. Almessiere, H. Sozeri, I. Ercan, M. Sertkol, S. Asiri, A Manikandan, Effect of annealing temperature on Magnetic and Mossbauer properties of $ZnFe_2O_4$ nanoparticles by sol-gel approach, J. Supercond. Nov. Magn. 31 (2018) 3347–3356.

[8]. I. J. C. Lynda, M. Durka, A. Dinesh, A. Manikandan, S. K. Jaganathan, A. Baykal, S. Arul Antony, Enhanced Magneto-optical and Photocatalytic

Properties of Ferromagnetic $Mg_{1-y}Ni_yFe_2O_4$ ($0.0 \leq y \leq 1.0$) Spinel Nano-ferrites, J. Supercond. Nov. Magn. 31 (2018) 3637–3647.

[9]. M. Maria Lumina Sonia, S. Anand, V. Maria Vinosel, M. Asisi Janifer, S. Pauline, A. Manikandan, Effect of lattice strain on structure, morphology and magneto-dielectric properties of $NiGd_xFe_{2-x}O_4$ ferrite nano-crystallites synthesized by sol-gel route, J. Magn. Magn. Mater. 466 (2018) 238-251.

[10]. A. Godlyn Abraham, A. Manikandan, E. Manikandan, S. K. Jaganathan, A. Baykal, P. Sri Renganathan, Enhanced Opto-Magneto Properties of $Ni_xMg_{1-x}Fe_2O_4$ ($0.0 \leq x \leq 1.0$) Ferrites Nano-Catalysts, J. Nanoelect. Optoelect. 12 (2017) 1326–1333

[11]. S. Asiri, M. Sertkol, S. Guner, H. Gungunes, K.M. Batoo, T.A. Saleh, H. Sozeri, M.A. Almessiere, A. Manikandan, A. Baykal, Hydrothermal synthesis of $Co_yZn_yMn_{1-2y}Fe_2O_4$ nanoferrites: Magneto-optical investigation, Ceram. Int. 44 (2018) 5751–5759.

[12]. A. Baykal, S. Guner, H. Gungunes, K.M. Batoo, Md. Amir, A. Manikandan, Magneto Optical Properties and hyperfine interactions of Cr^{3+} ion substituted copper ferrite nanoparticles, J. Inorg. Organomet. Polym. 28 (2018) 2533–2544,

[13]. E. Hema, A. Manikandan, P. Karthika, M. Durka, S. Arul Antony, B. R. Venkatraman, Magneto-optical properties of recyclable spinel $Ni_xMg_{1-x}Fe_2O_4$ ($0.0 \leq x \leq 1.0$) nano-catalysts, J. Nanosci. Nanotech. 16 (2016) 7325-7336.

[14]. Y. Slimani, A. Baykal, Md. Amir, N. Tashkandi, H. Güngüneş, S. Guner, H.S. El Sayed, F. Aldakheel, T.A. Saleh, A. Manikandan, Substitution effect of Cr^{3+} on hyperfine interactions, magnetic and optical properties of Sr-hexaferrites, Ceram. Int. 44 (2018) 15995-16004.

[15]. Y. Slimani, H. Gungunes, M. Nawaz, A. Manikandan, H.S. El Sayed, M.A. Almessiere, H. Sozeri, S.E. Shirsath, I. Ercan, A. Baykal, Magneto-optical and microstructural properties of spinel cubic copper ferrites with Li-Al co-substitution, Ceram. Int. 44 (2018) 14242-14250.

[16]. S. Asiri, S. Güner, A. Demir, A. Yildiz, A. Manikandan, A. Baykal, Synthesis and Magnetic Characterization of Cu Substituted Barium Hexaferrites, J. Inorg. Organomet. Polym. Mater. 28 (2018) 1065–1071.

[17]. A. Silambarasu, A. Manikandan, K. Balakrishnan, Room temperature superparamagnetism and enhanced photocatalytic activity of magnetically reusable spinel $ZnFe_2O_4$ nano-catalysts, J. Supercond. Nov. Magn. 30 (2017) 2631–2640.

[18]. G. Padmapriya, A. Manikandan, V. Krishnasamy, S. K. Jaganathan, S. Arul Antony, Enhanced catalytic activity and magnetic properties of spinel $Mn_xZn_{1-x}Fe_2O_4$ ($0.0 \leq x \leq 1.0$) nano-photocatalysts by microwave irradiation route, J. Supercond. Nov. Magn. 29 (2016) 2141-2149.

[19]. S. Gunasekaran, K. Thanrasu, A. Manikandan, M. Durka, A. Dinesh, S. Anand, S. Shankar, Y.Slimani, M. A. Almessiere, A. Baykal, Structural, fabrication and enhanced electromagnetic wave absorption properties of reduced graphene oxide (rGO)/zirconium substituted cobalt ferrite ($Co_{0\cdot5}Zr_{0\cdot5}Fe_2O_4$) nanocomposites, Physica B: Condensed Matter, 605 (2021) 412784.

[20]. F. Hussain, S. Z. Shah, H. Ahmad, S. A. Abubshait, H. A. Abubshait, A. Laref, A. Manikandan, H. S. Kusuma, M. Iqbal, Microalgae an ecofriendly and sustainable wastewater treatment option: Biomass application in biofuel and bio-fertilizer production. A review, Renewable and Sustainable Energy Reviews, 137 (2021) 110603.

[21]. P. A. Vinosha, A. Manikandan, A. S. J. Ceicilia, A. Dinesh, G. F. Nirmala, A. Christy Preetha, Y. Slimani, M.A. Almessiere, A. Baykal, B. Xavier, Review on recent advances of zinc substituted cobalt ferrite nanoparticles: Synthesis characterization and diverse applications, Ceramics International, 47 (2021) 10512-10535.

[22]. S. Blessi, S. Anand, A. Manikandan, M. M. Lumina Sonia, V. Maria Vinosel, Y. Slimani, M.A. Almessiere, A. Baykal, Structural, optical and electrochemical

investigations of Sb substituted mesoporous SnO_2 nanoparticles, Journal of Materials Science: Materials in Electronics, 32 (2021) 4132–4145.

[23]. Y. Slimani, N. A. Algarou, M. A. Almessiere, A. Sadaqat M. G. Vakhitov, D. S. Klygach, D. I. Tishkevich, A. V. Trukhanov, S. Güner, A. S. Hakeem, I. A. Auwal, A. Baykal, A. Manikandan, I. Ercan, Fabrication of exchanged coupled hard/soft magnetic nanocomposites: Correlation between composition, magnetic, optical and microwave properties, Arabian Journal of Chemistry, 10 (2021) 102992.

[24]. P. Manimaran, S. Balasubramaniyan, M. Azam, D. Rajadurai, S. I. Al-Resayes, G. Mathubala, A. Manikandan, S. Muthupandi, Z. Tabassum, I. Khan, Synthesis, Spectral Characterization and Biological Activities of Co(II) and Ni(II) Mixed Ligand Complexes, Molecules, 26 (2021) 823.

[25]. O. Alagha, N. Ouerfelli, H. Kochkar, M. A. Almessiere , Y. Slimani, A. Manikandan, A. Baykal, A. Mostafa, M. Zubair, M. H. Barghouthi, Kinetic Modeling for Photo-Assisted Penicillin G Degradation of $(Mn_{0.5}Zn_{0.5})[Cd_xFe_{2-x}]O_4$ ($x \leq 0.05$) Nanospinel Ferrites, Nanomaterials, 11 (2021) 970.

[26]. M. R. Ranjitha, A. Manikandan, J. N. Baby, K. Panneerselvam, S. Ragu, Mary George, Y. Slimani, M.A. Almessiere, A. Baykal, Hexagonal basalt-like ceramics $La_xMg_{1-x}TiO_3$ (x = 0 and 0.5) contrived via deep eutectic solvent for selective electrochemical detection of dopamine, Physica B: Condensed Matter, 615 (2021) 413068.

[27]. M. A. Almessiere, B. Unal, I.A. Auwal, Y. Slimani, H. Aydin, A. Manikandan, A. Baykal, Impact of calcination temperature on electrical and dielectric properties of $SrGa_{0.05}Fe_{11.98}O_4$-$Zn_{0.5}Ni_{0.5}Fe_2O_4$ hard/soft nanocomposites, Journal of Materials Science: Materials in Electronics, 32 (2021) 16589-16600.

[28]. K. Geetha, R. Udhayakumar, A. Manikandan, Enhanced magnetic and photocatalytic characteristics of cerium substituted spinel $MgFe_2O_4$ ferrite nanoparticles, Physica B: Physics of Condensed Matter, 615 (2021) 413083.

[29]. S. S. Al-Jameel, S. Rehman, M. A. Almessiere, F. A. Khan, Y. Slimani, N. S. Al-Saleh,
A. Manikandan, E. A. Al-Suhaimi, A. Baykal, Anti-microbial and anti-cancer activities of $MnZnDy_xFe_{2-x}O_4$ ($x \leq 0.1$) nanoparticles, Artificial Cells, Nanomedicine and Biotechnology, 49 (2021) 493-499.

[30]. S. Rehman, M. A. Almessiere, S. S. Al-Jameel, U. Ali, Y. Slimani, N. Taskhandi, N. S. Al-Saleh, A. Manikandan, F. A. Khan, E. A. Al-Suhaimi, A. Baykal, Designing of $Co_{0.5}Ni_{0.5}Ga_xFe_{2-x}O_4$ ($0.0 \leq x \leq 1.0$) Microspheres via Hydrothermal Approach and Their Selective Inhibition on the Growth of Cancerous and Fungal Cells, Pharmaceutics, 13 (2021) 962.

[31]. M. A. Almessiere, B. Unal, Y. Slimani, H. Gungunes, M. S. Toprak, N. Tashkand, A. Baykal, M. Sertkol, A.V. Trukhanov, A. Yıldız, A. Manikandan, Effects of Ce-Dy rare earths co-doping on various features of Ni-Co spinel ferrite microspheres prepared via hydrothermal approach, J. of Materials Research and Technology, 14 (2021) 2534-2553.

[32]. S. Blessi, A. Manikandan, S. Anand, M. M. L. Sonia, V. M. Vinosel, P. Paulraj, Y. Slimani, M.A. Almessiere, M. Iqbal, S. Guner, A. Baykal, Effect of Zinc substitution on the physical and electrochemical properties of mesoporous SnO_2 nanomaterials, Materials Chemistry and Physics, 273 (2021) 125122.

[33]. M. A. Almessiere, Y. Slimani, Y. O. Ibrahim, M. A. Gondal, M. A. Dastageer, I. A. Auwal, A. V. Trukhanov, A. Manikandan, A. Baykal, Morphological, structural, and magnetic characterizations of hard-soft ferrite nanocomposites synthesized via pulsed laser ablation in liquid, Materials Science and Engineering B, 273 (2021) 115446.

[34]. S. Blessi, S. Anand, A. Manikandan, M. Maria Lumina Sonia, V. Maria Vinosel, Y. Slimani, M.A. Almessiere, A. Baykal, Influence of Ni substitution on opto-magnetic and electrochemical properties of CTAB capped mesoporous SnO_2 nanoparticles, Journal of Materials Science: Materials in Electronics, Journal of Materials Science: Materials in Electronics, 32 (2021) 7630–7646.

[35]. M. George, T.L. Ajeesha, A. Manikandan, Ashwini Anantharaman, R.S. Jansi, E. Ranjith Kumar, Y. Slimani, M.A. Almessiere, A. Baykal, Evaluation of Cu-$MgFe_2O_4$ spinel nanoparticles for photocatalytic and antimicrobial activates, Journal of Physics and Chemistry of Solids, 153 (2021) 110010.

[36]. S. S. Al-Jameel, M. A. Almessiere, F. A. Khan, N. Taskhandi , Y. Slimani, N. S. Al-Saleh, A. Manikandan, E. A. Al-Suhaimi, A. Baykal, Synthesis, Characterization, Anti-Cancer Analysis of $Sr_{0.5}Ba_{0.5}Dy_xSm_xFe_{8-2x}O_{19}$ ($0.00 \leq x \leq 1.0$) Microsphere Nanocomposites, Nanomaterials, 11 (2021) 700.